QCD NLO corrections to inclusive B_c^* production in Z^0 decays

Jun Jiang,[1,*] Long-Bin Chen,[1,†] and Cong-Feng Qiao[1,2,‡]

[1]*School of Physics, University of Chinese Academy of Sciences, YuQuan Road 19A, Beijing 100049, China*
[2]*CAS Center for Excellence in Particle Physics, Beijing 100049, China*

We calculate the next-to-leading order (NLO) quantum chromodynamics (QCD) corrections to the inclusive process of $Z_0 \to B_c^* + \bar{c} + b$ under the nonrelativistic QCD (NRQCD) factorization scheme. Technical details about contributions from vector and axial-vector currents in a dimensional regularization scheme are discussed. Numerical calculation shows that the NLO correction enhances the leading-order decay width by about 50%, and the dependence on renormalization scale μ is reduced. The uncertainties induced by quark masses and the renormalization scale μ are also analyzed.

PACS numbers: 13.85.Ni, 14.40.Nd, 12.39.Jh, 12.38.Bx

I. INTRODUCTION

Due to its unique nature in the family of mesons, the B_c system attracts wide attention in experiments and theory. The study of B_c mesons may deepen our understanding of the Standard Model (SM) and the effective theory, non-relativistic quantum chromodynamics (NRQCD) [1]. The B_c meson was first discovered at the Fermilab TEVATRON [2], and its excited state $B_c(2S)$ [3] was recently observed by the ATLAS Collaboration.

For B_c meson direct production, various investigations had been carried out. The authors of Refs. [4–7] studied in detail the B_c hadroproduction, in which the P-wave [5] and color-octet [6] contributions, as well as the "intrinsic heavy quark mechanism" [7], were taken into account. The authors of Refs. [8,9] discussed the B_c production through the fragmentation scheme, and a Monte Carlo simulation program [10] for the B_c hadroproduction was also produced.

Apart from the direct production, B_c meson indirect production is also interesting, which may inform us not only about the nature of the B_c meson, but also the characters of its parent particles. The authors of Refs. [11,12] discussed B_c production through the top quark decays, those of Ref. [13] calculated production through $W^\pm$ decays, and those of Refs. [9,14,15] analyzed production through Z^0 decays. In the work of Ref. [16], the NLO QCD corrections to the $Z^0 \to B_c(^1S_0) + \bar{c} + b$ process was calculated.

At the LHC and International Linear Collider (ILC) [17], or other forms of Z factories, the Z^0 boson is and will be copiously produced. The Z^0 production cross section at the LHC is about 34 nb [18], and at the ILC, e.g., the cross section will be about 30 nb while the collider runs at the Z^0 pole energy [19]. Given the colliders' luminosity to be 10^{34} cm^{-2} s$^{-1} \approx 10^8$ nb^{-1}/year, there will be $\sim 10^9$ Z^0

events being produced per year at the LHC and ILC. Therefore, studying the B_c production in Z^0 decays is worthwhile and meaningful. Also, for this aim, since the B_c^* will almost completely decay to scalar B_c and the NLO QCD correction in the heavy quarkonium energy region is large, in some cases even huge, in this work we calculate the NLO QCD corrections for the $Z^0 \to B_c^*(^3S_1) + \bar{c} + b$ process.

The rest of the paper is organized as follows. In Sec. II we recalculate the Z^0 to B_c^* process at the Born level. In Sec. III, the NLO virtual and real QCD corrections to the leading order result are evaluated. Section IV presents some technical details of the calculation. In Sec. V, the numerical evaluation for the concerned decay process is performed at NLO accuracy. The last section is for summary and conclusions.

II. LEADING ORDER CONTRIBUTION

The $Z^0(k) \to B_c^*(p_0) + \bar{c}(p_5) + b(p_6)$ process starts from α_s^2 order, the Born level, and the corresponding four independent Feynman diagrams are shown in Fig. 1. The decay width may be expressed in a standard form, i.e.,

$$d\Gamma_{\text{Born}} = \frac{1}{2m_Z}\frac{1}{3}\sum |\mathcal{M}_{\text{Born}}|^2 d\text{PS}_3. \qquad (1)$$

Here, $\sum$ means summing over the polarizations and colors of final particles, 1/3 comes from the spin average of the initial state, and $d\text{PS}_3$ stands for the three-body phase space of final states, which can be explicitly expressed as

$$d\text{PS}_3 = \frac{1}{2^7 \pi^3 m_Z^2} ds_2 ds_1, \qquad (2)$$

where $s_1 = (p_0 + p_5)^2 = (k - p_6)^2$ and $s_2 = (p_5 + p_6)^2 = (k - p_0)^2$. The upper and lower bounds for s_1 and s_2 can be found in our previous work [16], or any standard textbook of particle physics.

---
*jiangjun13b@mails.ucas.ac.cn
†chenglogbin10@mails.ucas.ac.cn
‡qiaocf@ucas.ac.cn, corresponding author
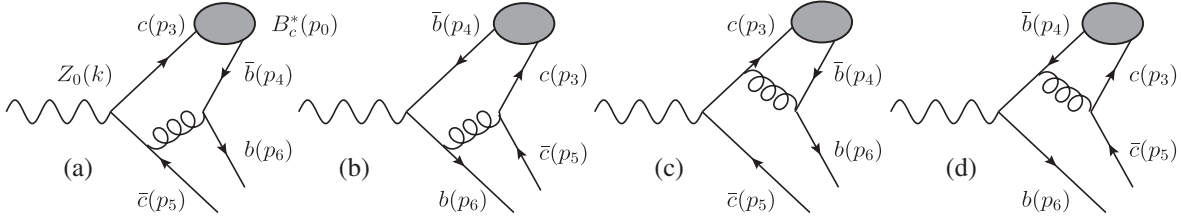
FIG. 1.   The leading order Feynman diagrams for B_c^* production in Z^0 decays.

The amplitude $M_{\text{Born}} = M_a + M_b + M_c + M_d$ can be readily obtained from Fig. 1 according to Feynman rules:

$$\mathcal{M}_a = \mathcal{C} \times \bar{u}(p_6)\gamma^\mu \frac{v(p_4)\bar{u}(p_3)}{(p_4+p_6)^2} \epsilon\!\!\!/(k)(T_c - \gamma^5) \frac{(-\not{p}_4 - \not{p}_5 - \not{p}_6) + m_c}{(-p_4 - p_5 - p_6)^2 - m_c^2} \gamma_\mu v(p_5),$$

$$\mathcal{M}_b = \mathcal{C} \times \bar{u}(p_6)\gamma^\mu \frac{(\not{p}_3 + \not{p}_5 + \not{p}_6) + m_b}{(p_3+p_5+p_6)^2 - m_b^2} \epsilon\!\!\!/(k)(\gamma^5 - T_b) \frac{v(p_4)\bar{u}(p_3)}{(p_3+p_5)^2} \gamma_\mu v(p_5),$$

$$\mathcal{M}_c = \mathcal{C} \times \bar{u}(p_6)\gamma^\mu \frac{v(p_4)\bar{u}(p_3)}{(p_4+p_6)^2} \gamma_\mu \frac{(\not{p}_3 + \not{p}_4 + \not{p}_6) + m_c}{(p_3+p_4+p_6)^2 - m_c^2} \epsilon\!\!\!/(k)(T_c - \gamma^5)v(p_5),$$

$$\mathcal{M}_d = \mathcal{C} \times \bar{u}(p_6)\epsilon\!\!\!/(k)(\gamma^5 - T_b) \frac{(-\not{p}_3 - \not{p}_4 - \not{p}_5) + m_b}{(-p_3 - p_4 - p_5)^2 - m_b^2} \gamma^\mu \frac{v(p_4)\bar{u}(p_3)}{(p_3+p_5)^2} \gamma_\mu v(p_5). \tag{3}$$

Here, the constant $\mathcal{C} = \frac{\pi \alpha_s g C_F}{\cos \theta_W}$ with θ_W being the Weinberg angle, $\epsilon(k)$ is the polarization vector of Z^0 boson, $T_c = (1 - \frac{8}{3}\sin^2\theta_W)$, and $T_b = (1 - \frac{4}{3}\sin^2\theta_W)$. For c and $\bar{b}$ constituent quarks hadronization to B_c^* meson, the following projection operator is employed [20]:

$$v(p_4)\bar{u}(p_3) \rightarrow \frac{\Psi_{3S_1}(0)}{2\sqrt{m_{B_c^*}}} \epsilon^*(p_0)(\not{p}_0 + m_{B_c^*}) \otimes \left(\frac{\mathbf{1}_c}{\sqrt{N_c}}\right), \tag{4}$$

where $\epsilon^*(p_0)$ is the polarization vector of B_c^* meson with $p_0 = p_3 + p_4$, $m_{B_c^*} = m_c + m_b$, $\mathbf{1}_c$ stands for the unit color matrix, and $\Psi_{3S_1}(0)$, a nonperturbative parameter, is the Schrödinger wave function at the origin of the B_c^* meson.

III. NEXT-TO-LEADING ORDER CORRECTIONS

The NLO QCD corrections to the $Z^0(k) \rightarrow B_c^*(p_0) + \bar{c}(p_5) + b(p_6)$ process contain virtual and real corrections, i.e., Γ_{Virtual} and Γ_{Real}, respectively, which are both at the order of α_s^3. Typical Feynman diagrams which are attributed

to the virtual correction are presented in Figs. 2–5, while those for the real correction are shown in Fig. 6. Note that in Figs. 3–6 only those diagrams with $Z \rightarrow \bar{c}c$ vertex have been displayed; the remaining half can easily be obtained by exchanging the c and b quark lines.

A. The virtual correction

With virtual correction, the decay width can be formulated as

$$d\Gamma_{\text{Virtual}} = \frac{1}{2m_Z} \frac{1}{3} \sum 2\text{Re}(\mathcal{M}_{\text{Virtual}} \mathcal{M}_{\text{Born}}^*) dPS_3. \tag{5}$$

In $\text{Re}(\mathcal{M}_{\text{Virtual}} \mathcal{M}_{\text{Born}}^*)$, both ultraviolet (UV) and infrared (IR) divergences exist. The conventional dimensional regularization scheme with $D = 4 - 2\epsilon$ is adopted to regularize them. There are also Coulomb divergences, which in this work are factorized out through the threshold expansion technique [21] and then attributed to the bound state wave function. In the calculation, the NRQCD short distance coefficients are obtained by matching to the full
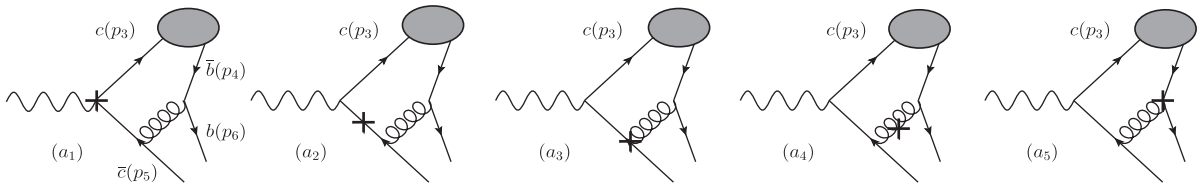
FIG. 2.   The typical counterterm Feynman diagrams corresponding to Fig. 1(a).
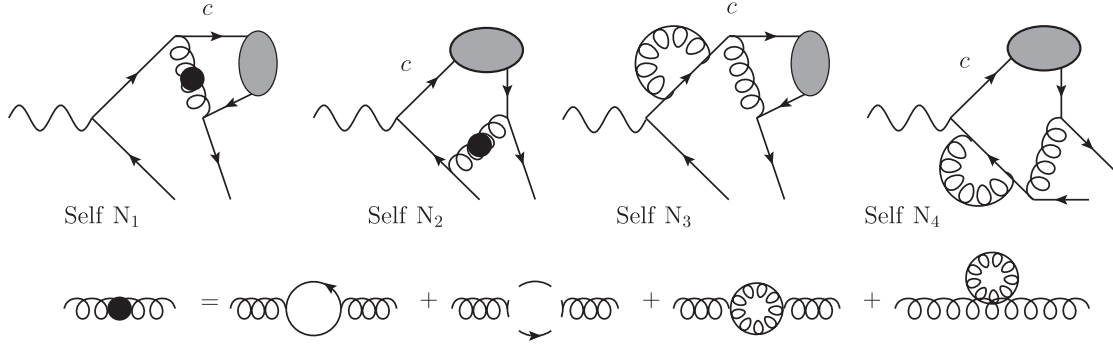
FIG. 3. Half of the self-energy diagrams in the virtual correction.
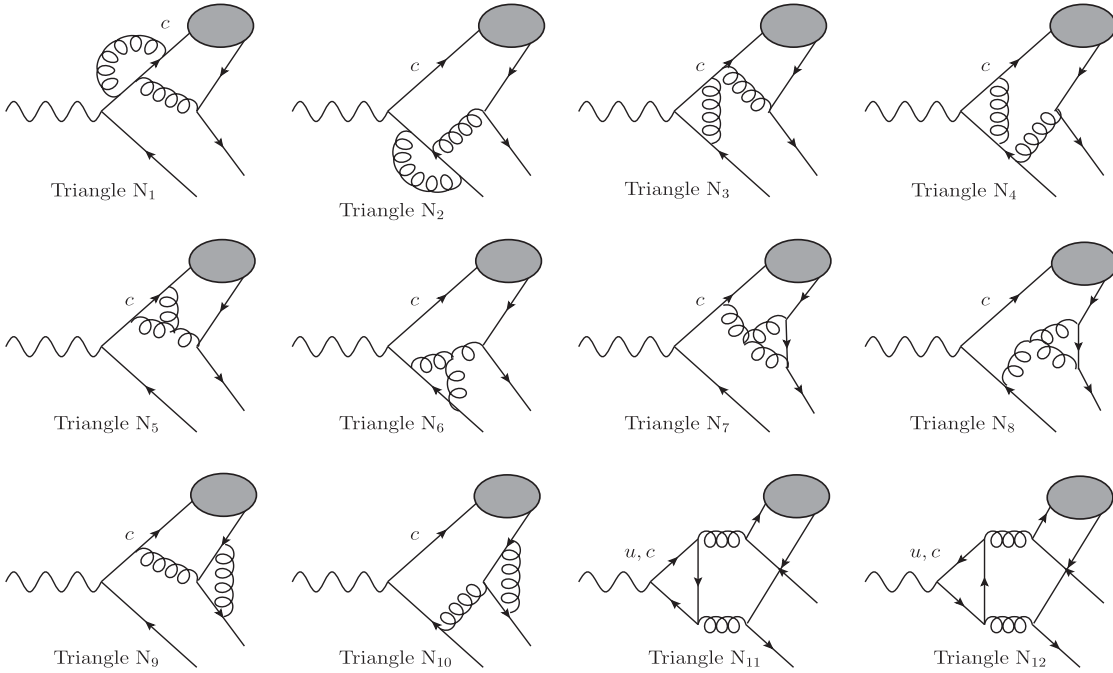
FIG. 4. Half of the triangle diagrams in the virtual correction.

QCD result stemming solely from the hard interaction region, and other regions give no contribution.

According to the power counting rule, the UV divergences exist merely in self-energy and triangle diagrams, which are canceled by counterterms (CT). Figure 2 contains 5 typical CT diagrams corresponding to Fig. 1(a), and hence there should be other 15 CT diagrams not shown. Of the 20 CTs, the renormalization constants include Z_2, Z_3, Z_m, and Z_g, corresponding to the renormalizations of quark field, gluon field, quark mass, and strong coupling constant α_s, respectively. In practice, the terms related to Z_3 vanish; e.g., those that contribute to Z_3 in Fig. 2, the (a_3) (a_4) and (a_5) cancel with one another. In the calculation, Z_g is defined in the modified-minimal-subtraction ($\overline{\text{MS}}$) scheme, while for Z_2 and Z_m we take the on shell (OS). At the end of the day we have

$$\delta Z_2^{\text{OS}} = -C_F \frac{\alpha_s}{4\pi} \left[\frac{1}{\epsilon'_{\text{UV}}} + \frac{2}{\epsilon'_{\text{IR}}} - 3\ln(m^2) + 4 \right] + \mathcal{O}(\alpha_s^2),$$

$$\delta Z_m^{\text{OS}} = -3C_F \frac{\alpha_s}{4\pi} \left[\frac{1}{\epsilon'_{\text{UV}}} - \ln(m^2) + \frac{4}{3} \right] + \mathcal{O}(\alpha_s^2),$$

$$\delta Z_g^{\overline{\text{MS}}} = -\frac{\beta_0}{2} \frac{\alpha_s}{4\pi} \left[\frac{1}{\epsilon'_{\text{UV}}} - \ln(\mu^2) \right] + \mathcal{O}(\alpha_s^2). \tag{6}$$

Here, $1/\epsilon'_{\text{UV(IR)}} = 1/\epsilon - \gamma_E + \ln(4\pi\mu^2)$, μ is the renormalization scale, and the mass m in δZ_2^{OS} and δZ_m^{OS} stands for m_c and m_b accordingly, $\beta_0 = (11/3)C_A - (4/3)T_f n_f$ is the one-loop coefficient of the QCD beta function with $n_f = 5$, the number of active quarks in our calculation. Eventually, the UV divergences appearing in CTs eliminate all UV divergences in self-energy and triangle diagrams, leading to
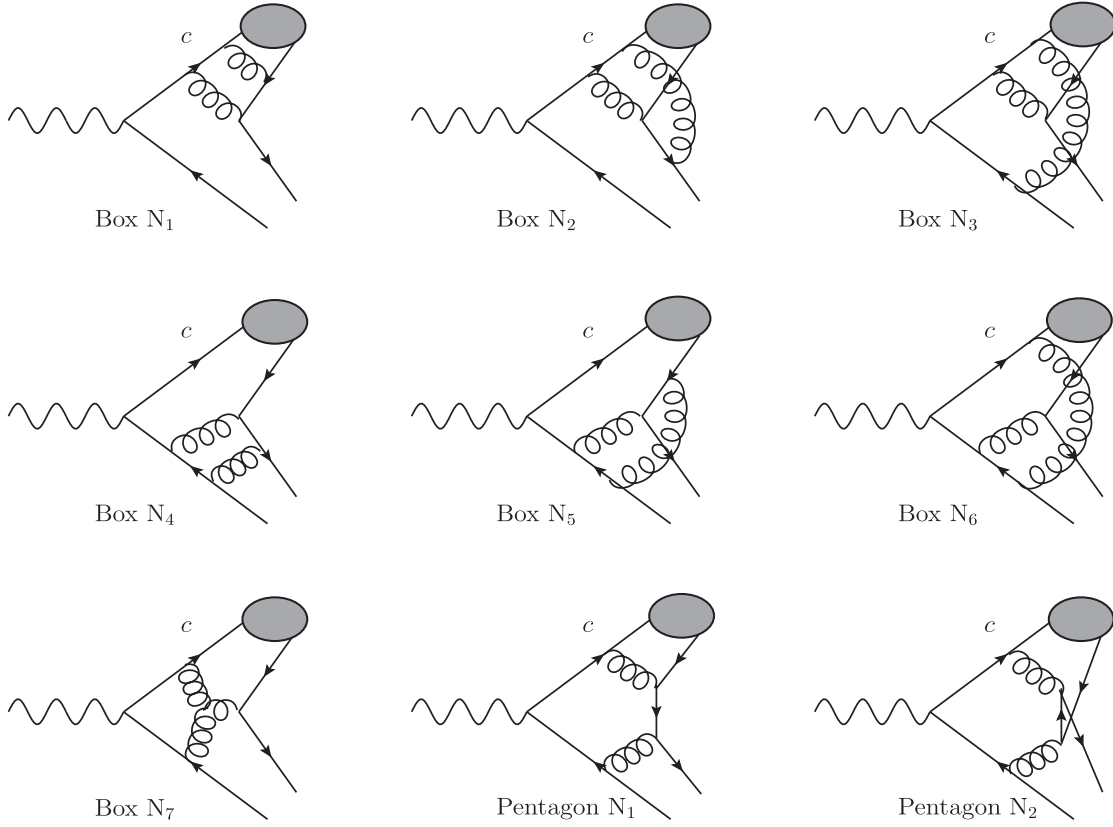
FIG. 5.   Half of the box and pentagon diagrams in the virtual correction.

a UV-free result. The remaining IR divergences in CTs have the following form:

$$d\Gamma_{\text{CT}}^{\text{IR}} = -\frac{2C_F \alpha_s}{\pi \epsilon_{\text{IR}}'} d\Gamma_{\text{Born}}. \tag{7}$$

In one-loop Feynman diagrams, the IR divergences involve triangle, box and pentagon diagrams. Of the triangle diagrams in Fig. 4, only two have IR divergences, i.e., Triangle N_9 and Triangle N_{10}. Of the diagrams in Fig. 5, Box N_7 has no IR divergences, Box N_1 and Pentagon N_1 have both Coulomb singularities and IR divergences, and the remaining other diagrams have only the IR divergences. We find that the cancellation of IR divergences in Figs. 4 and 5 goes as follows:

  (i) Combinations of Triangle N_9 + Box N_2, Box N_5 + Box N_6 are IR finite;
 (ii) Combinations of Triangle N_{10} + Box N_3 + Pentagon N_2 are IR finite;
(iii) The remaining IR divergences lie in Box N_1, Box N_4, and Pentagon N_1;
 (iv) Diagrams with the $Z \to \bar{b}b$ vertex have the same cancellation pattern as above.

B. The real correction

For the real correction of the concerned process, in which the IR divergences exist, there are 24 Feynman diagrams and half of them are shown in Fig. 6. To regularize the IR

singularities, the "two cutoff phase space slicing method" has been employed [22]. For diagrams contain IR divergences, we enforce a cut δ on the energy of the emitting gluon, the p_7^0. The gluon with energy $p_7^0 < \delta$ is considered to be soft, while $p_7^0 > \delta$ is treated as hard. Then, the decay width can be written as

$$d\Gamma_{\text{Real}} = d\Gamma_{\text{Real}}|_{\text{IR}} + d\Gamma_{\text{Real}}|_{\text{IR-free}},$$
$$d\Gamma_{\text{Real}}|_{\text{IR}} = d\Gamma_{\text{Real}}^{\text{IR-soft}}|_{p_7^0 < \delta} + d\Gamma_{\text{Real}}^{\text{IR-hard}}|_{p_7^0 > \delta}. \tag{8}$$

In Fig. 6, we find that
  (i) The first 4 diagrams, the Real $N_{1,2,3,4}$, are IR free;
 (ii) The combination of Real N_5 + Real N_6, Real N_7 + Real N_8 has no IR singularity;
(iii) The remaining 4 diagrams, i.e., Real $N_{9,10,11,12}$, have IR divergences;
 (iv) The diagrams with $Z \to \bar{b}b$ vertex behave the same as above.

Then the decay width in the soft sector $d\Gamma_{\text{Real}}^{\text{IR-soft}}|_{p_7^0 < \delta}$ can be written as

$$d\Gamma_{\text{Real}}^{\text{IR-soft}}|_{p_7^0 < \delta} = \frac{1}{2m_Z} \frac{1}{3} \sum |\mathcal{M}_{\text{Real}}^{\text{IR-soft}}|^2 \times d\text{PS}_4|_{\text{soft}}. \tag{9}$$

In the eikonal approximation, the squared amplitude $|\mathcal{M}_{\text{Real}}^{\text{IR-soft}}|^2$ reads
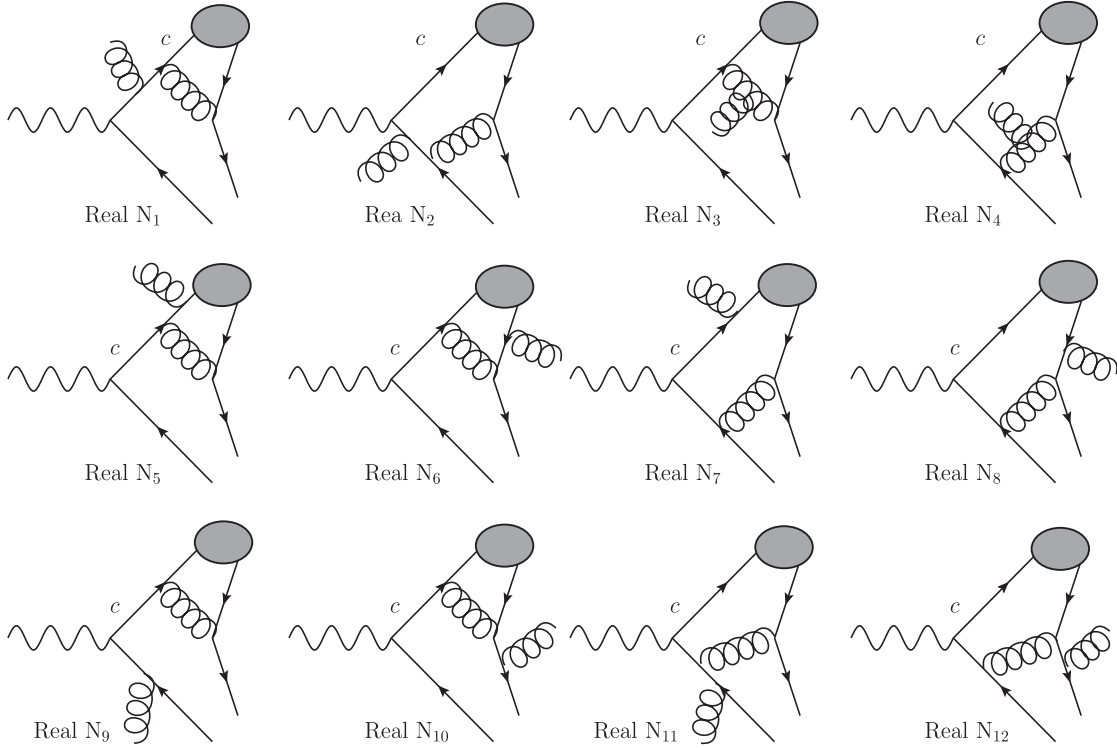
FIG. 6. Half of the Feynman diagrams in the real correction.

$$|\mathcal{M}_{\text{Real}}^{\text{IR}-\text{soft}}|^2 = -(C_F 4\pi\alpha_s)|\mathcal{M}_{\text{Born}}|^2 \times \left(\frac{p_5^2}{(p_5 \cdot p_7)^2} - 2\frac{p_5 \cdot p_6}{(p_5 \cdot p_7)(p_6 \cdot p_7)} + \frac{p_6^2}{(p_6 \cdot p_7)^2} \right), \tag{10}$$

which contains all the IR singularities in the real correction, i.e., Real $N_{9,10,11,12}$ and the other 4 diagrams with a $Z^0 \to \bar{b}b$ vertex. The four-body phase space in the soft sector possesses the form

$$d\text{PS}_4|_{\text{soft}} = d\text{PS}_3 \frac{d^3 p_7}{(2\pi)^3 2p_7^0}|_{p_7^0 < \delta}. \tag{11}$$

Finally in the small δ limit, the $d\Gamma_{\text{Real}}^{\text{IR}-\text{soft}}|_{p_7^0 < \delta}$ can be expressed as

$$d\Gamma_{\text{Real}}^{\text{IR}-\text{soft}}|_{p_7^0 < \delta} = d\Gamma_{\text{Born}} \frac{C_F \alpha_s}{\pi} \left(\frac{1}{\epsilon_{\text{IR}}'} - \ln(\delta^2) \right) \left(1 - \frac{\ln\frac{1+x_s}{1-x_s}}{2x_s} \right) + \text{finite terms} \tag{12}$$

with $x_s = \sqrt{1 - \frac{4mb^2mc^2}{(s_2 - mb^2 - mc^2)^2}}$. Here, those $1/\epsilon_{\text{IR}}'$ involved terms in (12) will cancel the IR singularities in CTs, i.e., (7), and those remaining ones in the one-loop Feynman diagrams. Note that the $\ln(\delta^2)$ involved terms will be canceled by the δ-dependent terms in the hard sector. In the end, the final result will be IR finite.

In the case of hard gluons, the decay width reads

$$d\Gamma_{\text{Real}}^{\text{IR}-\text{hard}}|_{p_7^0 > \delta} = \frac{1}{2m_Z}\frac{1}{3}\sum |\mathcal{M}_{\text{Real}}^{\text{IR}-\text{hard}}|^2 d\text{PS}_4|_{\text{hard}}. \tag{13}$$

Here in $|\mathcal{M}_{\text{Real}}^{\text{IR}-\text{hard}}|^2$, the radiation gluon is considered to be hard, and the phase space $d\text{PS}_4|_{\text{hard}}$ can be expressed as

$$\int d\text{PS}_4|_{\text{hard}} = \frac{2}{(4\pi)^6}\frac{\sqrt{(sy - m_c^2 - m_b^2)^2 - 4m_c^2 m_b^2}}{y}\int_{m_{B_c^*}}^{\frac{\sqrt{s}}{2}} dp_0^0 \int_{-1}^{1} d\cos\theta_c \int_0^{2\pi} d\phi_c$$

$$\times \left\{ \int_\delta^{p_{7-}^0} dp_7^0 \int_{y_-}^{y_+} dy + \int_{p_{7-}^0}^{p_{7+}^0} dp_7^0 \int_{\frac{(m_{B_c^*})^2}{s}}^{y_+} dy \right\}, \tag{14}$$

with

$$p_{7+}^0 = \frac{s - 2\sqrt{s}\,p_0^0}{2(\sqrt{s} - p_0^0 - |\vec{p_0}|)},$$

$$p_{7-}^0 = \frac{s - 2\sqrt{s}\,p_0^0}{2(\sqrt{s} - p_0^0 + |\vec{p_0}|)},$$

$$y_+ = \frac{1}{s}[(\sqrt{s} - p_0^0 - p_7^0)^2 - |\vec{p_0}|^2 - (p_7^0)^2 + 2|\vec{p_0}|p_7^0],$$

$$y_- = \frac{1}{s}[(\sqrt{s} - p_0^0 - p_7^0)^2 - |\vec{p_0}|^2 - (p_7^0)^2 - 2|\vec{p_0}|p_7^0].$$

$$(15)$$

Here, y is a dimensionless parameter defined as $y = (k - p_0 - p_7)^2/s$, $|\vec{p_0}| = \sqrt{(p_0^0)^2 - (m_{B_c^*})^2}$, and $\sqrt{s} = m_Z$.

The IR-free decay width with real correction can be formulated as

$$d\Gamma_{\text{Real}}|_{\text{IR−free}} = \frac{1}{2m_Z}\frac{1}{3}\sum|\mathcal{M}_{\text{Real}}^{\text{IR−free}}|^2 d\text{PS}_4, \quad (16)$$

where $|\mathcal{M}_{\text{Real}}^{\text{IR−free}}|^2$ is the amplitudes squared without IR singularities, and $d\text{PS}_4$ has exactly the same form of $d\text{PS}_4|_{\text{hard}}$ while $\delta = 0$. Finally, the sum of the soft and hard sectors, i.e., (12) and (13), together with the IR-free part (16), gives the full real correction.

In the end, with real and virtual corrections, one can readily obtain the total decay width for the inclusive process $Z^0(k) \to B_c^*(p_0) + \bar{c}(p_5) + b(p_6)$ at the NLO accuracy of QCD,

$$\Gamma_{\text{total}} = \Gamma_{\text{Born}} + \Gamma_{\text{Virtual}} + \Gamma_{\text{Real}} + \mathcal{O}(\alpha_s^4). \quad (17)$$

In (17), the decay width Γ_{total} is UV and IR finite, and the technical cut δ is independent as expected.

IV. SOME TECHNICAL DETAILS IN THE CALCULATION

In the conventional dimensional regularization scheme, the γ^5 problem needs to be handled carefully, especially in the process which contains the axial-vector current. In this work, we adopt the scheme given in Ref. [23], where the following rules are followed:

(I) The anticommutation relations, i.e., $\{\gamma^\mu, \gamma^5\} = 0$ and $\{\gamma^\mu, \gamma^\nu\} = 2g^{\mu\nu}$.

(II) The cyclicity is forbidden in traces involving odd number of γ^5. When several diagrams contribute to one process, one should write down the amplitudes starting from the same vertex, named the reading point.

(III) As a special case of rule II, in the anomalous axial-vector current situation, the reading point must be the axial-vector vertex in order to guarantee the conservation of the vector current.

When applying these rules to our process $Z^0(k) \to B_c^*(p_0) + \bar{c}(p_5) + b(p_6)$, some conclusions are obtained. That is, in the virtual correction, the amplitudes squared have the following two structures, schematically shown in Fig. 7:

Structure 1: The two $Z^0 - \bar{q}q$ vertexes lie in one fermion trace.

Structure 2: There are two fermion traces, each with a $Z^0 - \bar{q}q$ vertex and one involving a triangle anomalous diagram, e.g., Triangle N_{11} and Triangle N_{12} in Fig. 4.

For those whose amplitude squared belongs to Structure 1, since the amplitude can be separated into the vector part and the axial-vector part, amplitudes squared can be written as

$$\begin{aligned}
\text{Trace}[\mathcal{M}_{\text{Loop}}\mathcal{M}_{\text{Tree}}^\dagger] &= \text{Tr}[(\mathcal{M}_{\text{Loop}}^{\text{vector}} + \mathcal{M}_{\text{Loop}}^{\text{axial−vector}})(\mathcal{M}_{\text{Tree}}^{\text{vector}} + \mathcal{M}_{\text{Tree}}^{\text{axial−vector}})^\dagger] \\
&= \text{Tr}[\mathcal{M}_{\text{Loop}}^{\text{vector}}\mathcal{M}_{\text{Tree}}^{\text{vector}\dagger}] + \text{Tr}[\mathcal{M}_{\text{Loop}}^{\text{axial−vector}}\mathcal{M}_{\text{Tree}}^{\text{axial−vector}\dagger}] \\
&\quad + \text{Tr}[\mathcal{M}_{\text{Loop}}^{\text{vector}}\mathcal{M}_{\text{Tree}}^{\text{axial−vector}\dagger}] + \text{Tr}[\mathcal{M}_{\text{Loop}}^{\text{axial−vector}}\mathcal{M}_{\text{Tree}}^{\text{vector}\dagger}].
\end{aligned} \quad (18)$$
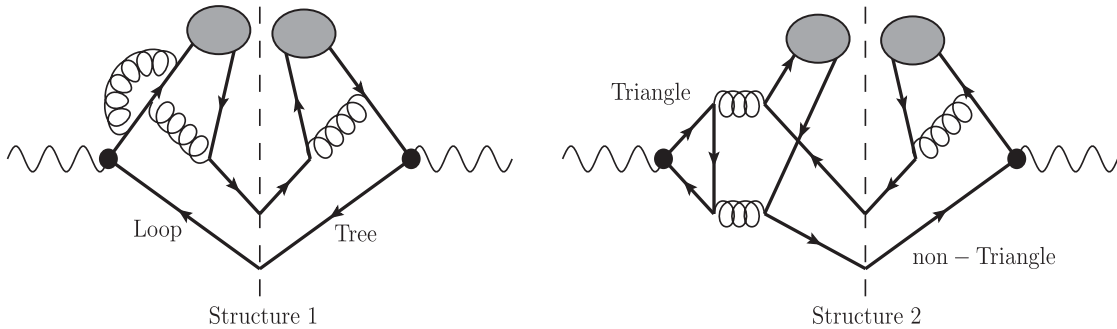
FIG. 7. Typical structures of the amplitudes squared of virtual correction.

In the last equation, though the first trace has no γ^5 and the second trace has two γ^5's, we can move them together by an anticommutation relation and contract them to unit 1; for the other two terms each has one γ^5, and they will be canceled by their own complex conjugate terms. As a result, there is no need to evaluate the last two traces in (18), and the calculation is hence greatly simplified.

For the triangle anomalous diagrams case, or amplitudes squared in Structure 2, as shown in Fig. 7, the amplitude squared reads

$$
\begin{aligned}
\mathcal{M}_{\text{Anomalous}}\mathcal{M}_{\text{Born}}^{\dagger} &= \text{Trace}[\mathcal{M}_{\text{Triangle}}]\text{Trace}[\mathcal{M}_{\text{non-Triangle}}] \\
&= \text{Tr}[\mathcal{M}_{\text{Triangle}}^{\text{vector}} + \mathcal{M}_{\text{Triangle}}^{\text{axial-vector}}]\text{Tr}[\mathcal{M}_{\text{non-Triangle}}^{\text{vector}} + \mathcal{M}_{\text{non-Triangle}}^{\text{axial-vector}}] \\
&= \text{Tr}[\mathcal{M}_{\text{Triangle}}^{\text{vector}}]\text{Tr}[\mathcal{M}_{\text{non-Triangle}}^{\text{vector}}] + \text{Tr}[\mathcal{M}_{\text{Triangle}}^{\text{vector}}]\text{Tr}[\mathcal{M}_{\text{non-Triangle}}^{\text{axial-vector}}] \\
&\quad + \text{Tr}[\mathcal{M}_{\text{Triangle}}^{\text{axial-vector}}]\text{Tr}[\mathcal{M}_{\text{non-Triangle}}^{\text{vector}}] + \text{Tr}[\mathcal{M}_{\text{Triangle}}^{\text{axial-vector}}]\text{Tr}[\mathcal{M}_{\text{non-Triangle}}^{\text{axial-vector}}].
\end{aligned}
\tag{19}
$$

Here in the last equation, the first term will be canceled by the one whose triangle fermion loop is reversed; i.e., the vector currents of Triangle N_{11} and Triangle N_{12} cancel with each other. The second and third terms will be canceled by their complex conjugate terms. The last term survives, and it is the only one we need to trace and contains one γ^5. In the final numerical calculation, the contribution coming from triangle anomalous diagrams turns out to be numerically insignificant.

In the case of real correction, since all the amplitudes squared have the same structure as Structure 1, one only needs to handle the Dirac traces without γ^5 or with two γ^5's.

In our calculation, the Mathematica package FeynArts [24] is used to generate the Feynman diagrams; FeynCalc [25] and FeynCalcFormLink [26] are used to handle the algebraic trace manipulation; $Apart [27] and FIRE [28], together with codes written by ourselves, are employed to reduce all the one-loop integrals into master integrals (A_0, B_0, C_0, D_0); and the LoopTools [29] is employed to calculate the master integrals numerically. The numerical integrations of the three- and four-body phase spaces are performed by VEGAS [30].

V. NUMERICAL RESULTS

For the numerical calculation, the following input parameters are used [31]:

$$
m_c = 1.5 \pm 0.1 \text{ GeV}, \qquad m_b = 4.9 \pm 0.2 \text{ GeV}, \qquad m_Z = 91.1876 \text{ GeV}, \qquad m_W = 80.399 \text{ GeV},
$$

$$
\sin^2\theta_W = 0.2312, \qquad g = 2\sqrt{2}m_W\sqrt{\frac{G_F}{\sqrt{2}}} = 0.6531, \qquad \Psi_{B_c^*}(0) = \frac{R(0)}{\sqrt{4\pi}} = 0.3615 \text{ GeV}^{\frac{3}{2}}.
\tag{20}
$$
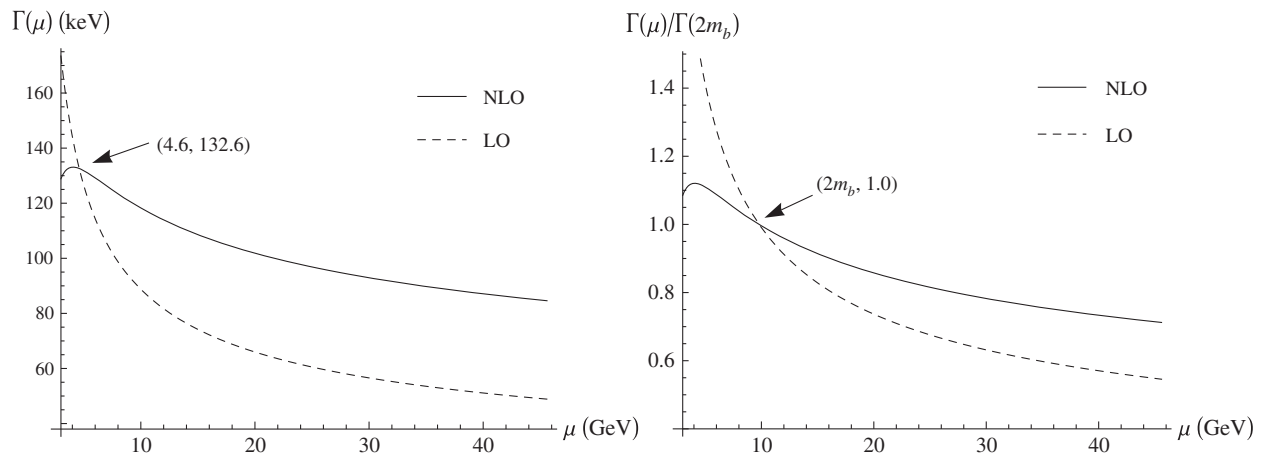
FIG. 8.   The decay width $\Gamma(\mu)$ and the ratio $\Gamma(\mu)/\Gamma(2m_b)$ versus renormalization scale μ for μ running from $2m_c$ to $m_Z/2$.

TABLE I. Decay widths $\Gamma(\mu)$ (keV) of $Z^0 \to B_c^* + \bar{c} + b$ at leading order and next-to-leading order. The first errors are caused by $m_c = 1.5 \pm 0.1$ GeV and the second ones by $m_b = 4.9 \pm 0.2$ GeV at $\mu = 2m_b$, 28 GeV, $m_Z/2$.

$\Gamma(\mu)$ (keV)	LO	NLO	K-factor
$\mu = 2m_b$	$89.56^{-17.10+0.71}_{+22.85-0.71}$	$118.77^{-23.11+0.37}_{+31.53+0.07}$	$1.33^{-0.01-0.01}_{+0.01+0.01}$
$\mu = 28$	$58.02^{-11.08+0.46}_{+14.80-0.46}$	$94.40^{-18.25+0.45}_{+24.73-0.22}$	$1.63^{-0.00-0.01}_{+0.01+0.01}$
$\mu = m_Z/2$	$48.87^{-9.33+0.39}_{+12.47-0.39}$	$84.60^{-16.33+0.44}_{+22.08-0.26}$	$1.73^{-0.00-0.00}_{+0.01+0.01}$

Here, G_F is the Fermi constant in weak interaction and $R(0)$ is the B_c^* meson's radial wave function at the origin, whose value is estimated via a potential model [32]. The two-loop strong coupling of

$$\frac{\alpha_s(\mu)}{4\pi} = \frac{1}{\beta_0 L} - \frac{\beta_1 \ln L}{\beta_0^3 L^2} \qquad (21)$$

is employed in the calculation, in which $L = \ln(\mu^2/\Lambda_{\text{QCD}}^2)$ with Λ_{QCD} being 214 MeV, and $\beta_1 = (34/3)C_A^2 - 4C_F T_F n_f - (20/3)C_A T_F n_f$ is the two-loop coefficient of the QCD beta function.

In Fig. 8, the decay width $\Gamma(\mu)$ and the ratio $\Gamma(\mu)/\Gamma(2m_b)$ versus renormalization scale μ are presented. The NLO corrections enhance the LO contribution to $Z^0 \to B_c^* + \bar{c} + b$ when $\mu > 4.6$ GeV. We can see from Fig. 8 that the renormalization scale dependence of the decay width is reduced evidently.

We adopt three typical renormalization scales in evaluation, and the corresponding values of the running coupling constant are $\alpha_s(\mu = 2m_b) = 0.1768$, $\alpha_s(\mu = 28 \text{ GeV}) = 0.1423$, and $\alpha_s(\mu = m_Z/2) = 0.1306$; the decay widths are as presented in Table I, where the first errors are induced by $m_c = 1.5 \pm 0.1$ GeV and the second ones are induced by $m_b = 4.9 \pm 0.2$ GeV. Here, the K-factor is defined as $\frac{\Gamma_{\text{NLO}}}{\Gamma_{\text{LO}}}$.

In the calculation, when we estimate the uncertainties induced by varying the m_c, the m_b is fixed and vice versa. The results of Table I indicate that

(i) The correction of NLO is significant, and the K-factor grows with the renormalization scale μ increase, yet it grows slower at the high scale region;

(ii) When renormalization scale μ increases, the decay widths for both LO and NLO decrease, yet both decrease slower at the high scale region;

(iii) The uncertainties caused by varying m_c are much larger than those induced by m_b.

To show the above results more clearly, in Fig. 9 we exhibit the LO (left) and NLO (right) decay widths with different quark masses versus running renormalization scale μ. It is obvious that the decay widths are much more sensitive to m_c than m_b; the three lines of $m_b = 4.9(\pm0.2)$ are very close to one another at both LO and NLO.

According to Ref. [16] and the above calculation, the B_c and $B_c^{(*)}$ production rates in Z^0 decays are readily obtained in LO and NLO, at scale $\mu = 2m_b$ for illustration. That is,

$$\text{Br}_{\text{LO}}(Z^0 \to B_c + \bar{c}b) = \frac{\Gamma_{\text{LO}}(B_c)}{\Gamma_Z} = 2.9 \times 10^{-5},$$

$$\text{Br}_{\text{NLO}}(Z^0 \to B_c + \bar{c}b) = \frac{\Gamma_{\text{NLO}}(B_c)}{\Gamma_Z} = 3.1 \times 10^{-5},$$

$$\text{Br}_{\text{LO}}(Z^0 \to B_c^* + \bar{c}b) = \frac{\Gamma_{\text{LO}}(B_c^*)}{\Gamma_Z} = 3.6 \times 10^{-5},$$

$$\text{Br}_{\text{NLO}}(Z^0 \to B_c^* + \bar{c}b) = \frac{\Gamma_{\text{NLO}}(B_c^*)}{\Gamma_Z} = 4.8 \times 10^{-5}, \qquad (22)$$

where $\Gamma_Z = 2.5$ GeV is the total decay width of Z^0 boson. Because the spin-triplet state B_c^* decays to the ground state B_c with an almost 100% rate, we obtain the total production rates for B_c production in Z^0 decay,
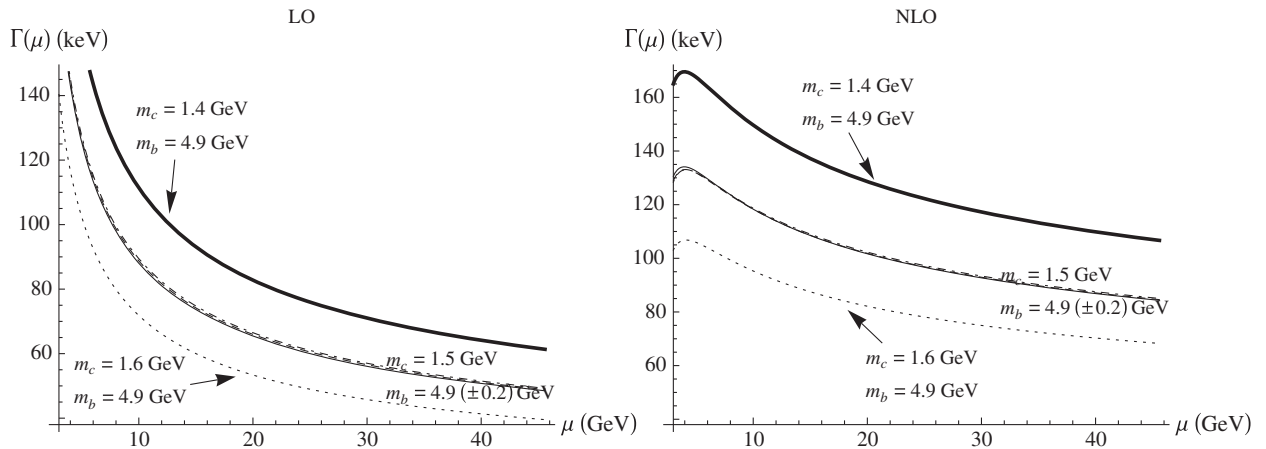
FIG. 9. The decay widths of LO (left) and NLO (right) with different quark masses versus running renormalization scale μ, from $2m_c$ to $m_Z/2$.

$$\mathrm{Br}_{\mathrm{LO}}(Z^0 \to B_c + X) = 6.5 \times 10^{-5},$$
$$\mathrm{Br}_{\mathrm{NLO}}(Z^0 \to B_c + X) = 7.9 \times 10^{-5}. \qquad (23)$$

Given about 10^9 or more Z^0 events being produced per year in future colliders, there would be sizable B_c's being produced. Also, the effects of the NLO corrections might be captured in experimental observation. It is worth noting that the LO contributions from the P-wave/color-octet are an order of magnitude smaller than those from the S-wave [15], which only enhance the total production rates slightly.

VI. SUMMARY AND CONCLUSIONS

In this work we calculated the decay width of the $Z^0 \to B_c^* + \bar{c} + b$ inclusive process at the NLO accuracy in the framework of NRQCD. The calculation procedures for both LO and NLO corrections were presented. Our analyses for the vector and axial-vector current contributions were performed in a dimensional regularization scheme. The decay width and its uncertainties caused by varying quark masses, as well as the dependence on renormalization scale μ, were presented numerically. Supposing that there will be copious Z^0 produced in future colliders, our calculation together with previous work [16] would be helpful for the precise study of B_c physics, and might also tell how well the perturbative calculation and nonrelativistic quark model work for the B_c system.

According to the calculation, the NLO QCD correction to the inclusive process $Z^0 \to B_c^* + \bar{c} + b$ is significant. We found that the renormalization scale μ dependence of the decay width is depressed while the NLO correction is taken into account. When the scale μ runs from $2m_b$ to $m_Z/2$, both values of Γ_{LO} and Γ_{NLO} decrease, yet the ratio $\Gamma_{\mathrm{NLO}}/\Gamma_{\mathrm{LO}}$ grows from 1.33 to 1.73, and the increasing trend slows down at high μ region. Moreover, the input parameter of quark mass m_c has a quite large influence on the decay width, for both Γ_{LO} and Γ_{NLO}, at both low and high μ regions as well. In contrast to m_c, the uncertainties induced by m_b are negligible.

[1] G. T. Bodwin, E. Braaten, and G. P. Lepage, Phys. Rev. D **51**, 1125 (1995); **55**, 5853(E) (1997).

[2] F. Abe *et al.* (CDF Collaboration), Phys. Rev. Lett. **81**, 2432 (1998); Phys. Rev. D**58**, 112004 (1998).

[3] G. Aad *et al.* (ATLAS Collaboration), Phys. Rev. Lett. **113**, 212004 (2014).

[4] C. H. Chang and Y. Q. Chen, Phys. Rev. D **48**, 4086 (1993); C. H. Chang, Y. Q. Chen, G. P. Han, and H. T. Jiang, Phys. Lett. B **364**, 78 (1995); K. Kolodziej, A. Leike, and R. Ruckl, Phys. Lett. B **355**, 337 (1995); C. H. Chang, Y. Q. Chen, and R. J. Oakes, Phys. Rev. D **54**, 4344 (1996); K. m. Cheung, Phys. Lett. B **472**, 408 (2000); C. H. Chang and X. G. Wu, Eur. Phys. J. C **38**, 267 (2004).

[5] C. H. Chang, J. X. Wang, and X. G. Wu, Phys. Rev. D **70**, 114019 (2004).

[6] C. H. Chang, C. F. Qiao, J. X. Wang, and X. G. Wu, Phys. Rev. D **71**, 074012 (2005).

[7] C. H. Chang, C. F. Qiao, J. X. Wang, and X. G. Wu, Phys. Rev. D **72**, 114009 (2005).

[8] E. Braaten, K. m. Cheung, and T. C. Yuan, Phys. Rev. D **48**, R5049 (1993).

[9] C. H. Chang and Y. Q. Chen, Phys. Rev. D **46**, 3845 (1992); **50**, 6013(E) (1994).

[10] C. H. Chang, C. Driouichi, P. Eerola, and X. G. Wu, Comput. Phys. Commun. **159**, 192 (2004); C. H. Chang, J. X. Wang, and X. G. Wu, Comput. Phys. Commun. **175**, 624 (2006).

[11] C. F. Qiao, C. S. Li, and K. T. Chao, Phys. Rev. D **54**, 5606 (1996); C. H. Chang, J. X. Wang, and X. G. Wu, Phys. Rev. D **77**, 014022 (2008); X. G. Wu, Phys. Lett. B **671**, 318 (2009).

[12] P. Sun, L. P. Sun, and C. F. Qiao, Phys. Rev. D **81**, 114035 (2010).

[13] C. F. Qiao, L. P. Sun, D. S. Yang, and R. L. Zhu, Eur. Phys. J. C **71**, 1766 (2011); Q. L. Liao, X. G. Wu, J. Jiang, Z. Yang, and Z. Y. Fang, Phys. Rev. D **85**, 014032 (2012).

[14] V. V. Kiselev, A. K. Likhoded, and M. V. Shevlyagin, Z. Phys. C **63**, 77 (1994); V. V. Kiselev, A. K. Likhoded, and M. V. Shevlyagin, Yad. Fiz. **57**, 733 (1994) [Phys. At. Nucl. **57**, 689 (1994)].

[15] L. C. Deng, X. G. Wu, Z. Yang, Z. Y. Fang, and Q. L. Liao, Eur. Phys. J. C **70**, 113 (2010); Z. Yang, X. G. Wu, L. C. Deng, J. W. Zhang, and G. Chen, Eur. Phys. J. C **71**, 1563 (2011).

[16] C. F. Qiao, L. P. Sun, and R. L. Zhu, J. High Energy Phys. 08 (2011) 131.

[17] G. Aarons *et al.* (ILC Collaboration), arXiv:0709.1893.

[18] S. Chatrchyan *et al.* (CMS Collaboration), Phys. Rev. Lett. **112**, 191802 (2014).

[19] J. Erler, S. Heinemeyer, W. Hollik, G. Weiglein, and P. M. Zerwas, Phys. Lett. B **486**, 125 (2000).

[20] A. Petrelli, M. Cacciari, M. Greco, F. Maltoni, and M. L. Mangano, Nucl. Phys. **B514**, 245 (1998).

[21] M. Beneke and V. A. Smirnov, Nucl. Phys. **B522**, 321 (1998).

[22] B. W. Harris and J. F. Owens, Phys. Rev. D **65**, 094032 (2002).

[23] J. G. Korner, D. Kreimer, and K. Schilcher, Z. Phys. C **54**, 503 (1992).

[24] T. Hahn, Comput. Phys. Commun. **140**, 418 (2001).

[25] R. Mertig, M. Bohm, and A. Denner, Comput. Phys. Commun. **64**, 345 (1991).

[26] F. Feng and R. Mertig, arXiv:1212.3522.

[27] F. Feng, Comput. Phys. Commun. **183**, 2158 (2012).

[28] A. V. Smirnov, J. High Energy Phys. 10 (2008) 107.

[29] T. Hahn and M. Perez-Victoria, Comput. Phys. Commun. **118**, 153 (1999).

[30] G. P. Lepage, CLNS-80/447.

[31] K. A. Olive *et al.* (Particle Data Group Collaboration), Chin. Phys. C **38**, 090001 (2014).

[32] E. J. Eichten and C. Quigg, Phys. Rev. D **49**, 5845 (1994).